Study of Microsegregation and Laves Phase in INCONEL718 Superalloy Regarding Cooling Rate During Solidification

LISHIBAO LING, YANFENG HAN, WEI ZHOU, HAIYAN GAO, DA SHU, JUN WANG, MAODONG KANG, and BAODE SUN

Cooling rate is an important and controllable variable in casting processing. The effect of cooling rate on the microsegregation and Laves phase in INCONEL718 superalloy castings was studied by high-temperature–laser confocal scanning microscopy and quantitative metallography in this study. The transformation rate of solid phase with a feature of Gaussian distribution in the solidifications at the cooling rates of 0.10 to 14 K/s is acquired. The solidification time and secondary dendrite arm spacing (SDAS) as a function of cooling rate are analyzed. The amount of Laves phase presents a maximum value at a threshold cooling rate of 3 K/s owing to the opposite effects of cooling rate on the solidification time and SDAS. A modified dimensionless microsegregation index criterion was used for the scaling of solute segregation and Laves phase depending on cooling rates. The prediction of maximal microsegregation and the amount of Laves phase by MSI and experiments provide a guide for cooling rate control in the casting applications.

I. INTRODUCTION

BASED on its good strength and excellent resistance to oxidation at elevated temperatures, INCONEL718,*

---

*INCONEL718 is a trademark of Special Metals Corporation, Huntington, WV.

---

a nickel-iron base and Nb-strengthened superalloy, is widely used for key structural castings in aircraft turbine.[1,2] In order to reduce the weight of aircraft turbine, complex thin-wall components of the INCONEL718 alloy are usually adopted and manufactured by investment casting.[3,4] Because of the positional variation and structural differences, the cooling rates of

LISHIBAO LING, WEI ZHOU, and MAODONG KANG, Ph.D. Candidates, are with the School of Materials Science and Engineering, Shanghai Jiao Tong University, No. 800 Dongchuan Road, Shanghai 200240, P.R. China. YANFENG HAN, Lecturer, HAIYAN GAO, Associate Professor, and DA SHU, Professor, are with the Shanghai Key Lab of Advanced High-temperature Materials and Precision Forming, Shanghai Jiao Tong University. Contact e-mail: yfhan@sjtu.edu.cn JUN WANG, Professor, is with the Shanghai Key Lab of Advanced High-temperature Materials and Precision Forming, Shanghai Jiao Tong University, also with the State Key Laboratory of Metal Matrix Composites, Shanghai Jiao Tong University, No. 800 Dongchuan Road, Shanghai 200240, P.R. China. BAODE SUN, Professor, Dean, is with the School of Materials Science and Engineering, Shanghai Jiao Tong University, also with the Shanghai Key Lab of Advanced High-temperature Materials and Precision Forming, Shanghai Jiao Tong University, also with the State Key Laboratory of Metal Matrix Composites, Shanghai Jiao Tong University.

whole castings vary locally. As a result, some solidification defects, such as solute segregation and undesirable Laves phase, randomly form during solidification. The segregation and Laves phase increase the hot tearing sensitivity of INCONEL718 alloy castings and harmfully influence their final properties owing to the depletion of potent solution strengthening elements for Ni-rich matrix.[5,6] Therefore, the cooling rate is one of the most important technological parameters that should be controlled during manufacturing complex thin-wall components.

It is known that the Laves phase is the product of a nonequilibrium eutectic reaction, $L \rightarrow \gamma + $ Laves, at the end of INCONEL718 alloy solidification, and its formation depends on the local nonequilibrium conditions of solidification and corresponding Nb redistribution.[7] Both experiment and modeling methods have been employed to investigate the solute concentration profile and eutectic phase along dendrite arms in the INCONEL718 microstructure.[8–10]

However, the cooling rate complicatedly influences solidification parameters, and it is difficult to establish a quantitative relationship between the cooling rate and the fraction of Laves phase in the eutectic region in the INCONEL718 castings. Bower et al.[11] and Flemings[12] proclaimed that the cooling rate has little effect on the degree of microsegregation and the amount of nonequilibrium eutectics. Antonsson and Fredriksson also indicated that the influence of cooling rate on the solidification microstructure at low or medium cooling rates could be negligible. However, the cooling rate significantly affects the Nb redistribution and the amount of Laves phase at high cooling rates. For example, no Laves phase was found in the alloys solidified at a very high cooling rate, ~5000 K/s, in the

levitation experiment.[13] In contrast, Nastac and Stefanescu[14–16] found that the solute redistribution and amounts of Laves phase are a function of the cooling rate and material parameters, and considered that the maximum amount of Laves phases is formed at a critical cooling rate. However, the growth of equiaxed dendritic grains within a spherical closed system was only considered as primary dendrite, and the range of cooling rates in the real investment casting was not fully covered. It is known that the formation of nonequilibrium eutectic phases is sensitive to the evolution of solid fraction in solidification. The precise calculation or experimental measurement of the solid fraction is crucial to studying the solute microsegregation in the interdendritic region. The purpose of this work is to study the microsegregation of solute Nb and Laves phase in eutectics as a function of cooling rates from 0.1 to 20 K/s, covering the range of cooling rates for major investment castings with INCONEL718 alloy based on in-situ solidification observation using a high-temperature–laser confocal scanning microscope (HT-LCSM, Lasertec Corporation, Japan).

II. EXPERIMENTAL DETAILS

A. Materials and Solidification Experiments

The INCONEL718 samples used in this study were extracted from a thin plate produced by the investment casting. The chemical compositions of INCONEL718 alloy, as given in Table I, were tested using an inductively coupled argon plasma–optical emission spectrometer (ICAP-OES 6000 Radial, Analytical West, Inc., USA) and high-frequency infrared ray carbon sulfur analyzer (CS-206, Baoying Technology, China). The extracted plates were ground and mechanically polished into thin discs with a diameter of 7 mm and height shorter than 0.5 mm to eliminate the temperature difference in the thickness direction following solidification.

The solidification experiments were performed on an HT-LCSM, which can be used for high-resolution in-situ metallography to distinguish solid from liquid phase at elevated temperatures up to 1873 K (1600 °C). The schematic diagram of the gold-plated ellipsoid infrared heating furnace chamber is shown in Figure 1(a), which shows that the chamber is similar to that in previous studies.[17–20] A halogen lamp (1.5 kW) was installed as a heating source at the lower focal point of the chamber and focused at the upper focal point of the chamber. The sample was put into a high-purity Al_2O_3 crucible and then placed at the upper focal point. The crucible was supported by a Pt sample holder, and one thermocouple was welded under the Pt sample holder to monitor and control the furnace temperature. The heating and cooling processes of the sample were controlled by the input power of a halogen lamp. After the gas in the chamber was evacuated, the chamber was continuously filled with ultrapurity argon (99.9996%) to prevent the oxidation of the sample surface at high temperature.

A pure Cr thin disc with a melting point up to 2073 K (1800 °C) was placed under the sample, as shown in Figure 1(b), to eliminate the influence of surface tension between the alloy liquid and crucible bottom on the surface flatness. The samples were heated to 1673 K (1400 °C) at a heating rate of 3 K/s and further held for 2 minutes to homogenize the liquid phase. Then the cooling was controlled at the rates of 0.10, 0.25, 0.50, 1.0, 2.0, 3.0, 4.0, 5.0, 6.0, 7.0, 10, 11, and 14 K/s, respectively. The accuracy of measured temperatures is very important in the HT-LCSM observation. Due to the nature of temperature control in the HT-LCSM, it is not possible to achieve exactly the target temperature during the rapid heating and cooling schedule. According to the reports of Yin and Emi[17] and Attallah et al.,[20] at low heating and cooling rates (<5 K/s), the difference between the measured temperature by a thermocouple and the real temperature on the upper surface of the sample is quite limited, ~7 K. Even at a higher heating rate, 20 K/s, the difference is ~20 K. The measured temperatures in this study have been carefully corrected according to the temperature calibration on the upper surface of the samples using an infrared thermometer.

B. Microstructural Characterization

After in-situ HT-LCSM observations, the solidified samples were mechanically polished and etched for 30 seconds in a mixture solution of 100 mL HCl, 100 mL CH_3CH_2OH, and 5 g $CuCl_2$. Their microstructures were analyzed with an optical microscope and field emission–scanning electron microscope (FE-SEM, JSM-7600F, JEOL, Japan) equipped with a backscattered electron detector and an energy-dispersive spectrometer (EDS). The fraction of Laves phase was characterized by the average value of more than 10 optical images at magnification 500 times using a commercial image analysis system (DT2000, Dongtu Digital Company, China). The secondary dendrite arm spacing (SDAS) in the final solidified microstructure was measured in the optical images using the linear intercept method.

III. RESULTS AND DISCUSSION

A. In-Situ Observation of Solidification Process

Figure 2 shows the recorded typical microstructures during the solidification at a cooling rate of 1 K/s. Since the sample is thin enough, its solidification can be regarded as an isothermal solidification wherein the nucleation uniformly happens in the alloy melts. With

Table I. Chemical Compositions of INCONEL718 Superalloy

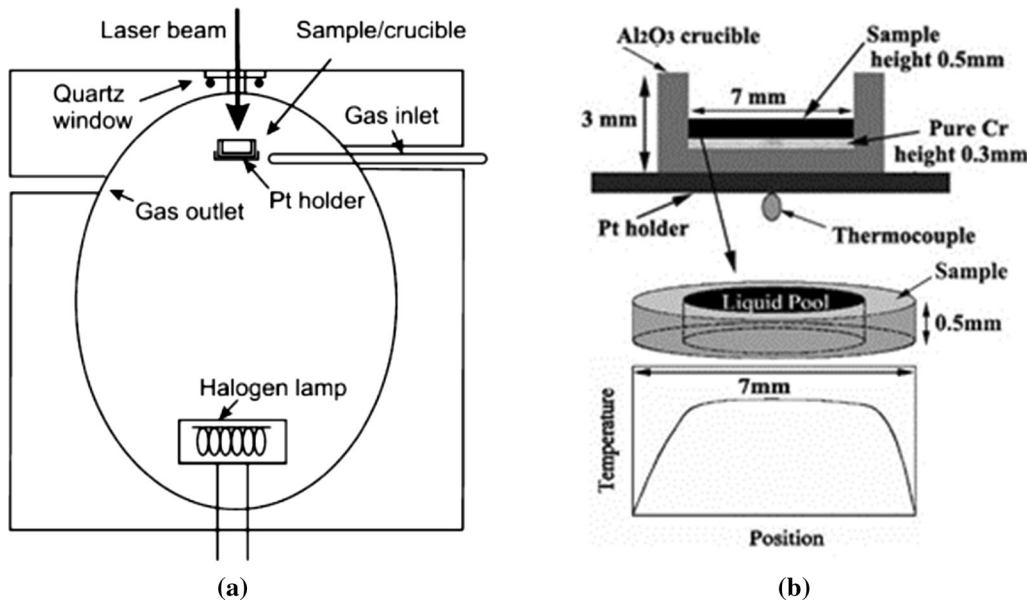| Elements	C	Si	P	Cr	Ni	Co	Mo	Al	Ti	Fe	Nb
Composition (wt pct)	0.06	0.189	0.003	19.45	52.09	0.18	3.15	0.41	1.06	18.58	4.82

Fig. 1—(a) Schematic diagram of the high-temperature cell of the LCSM. (b) Schematic diagrams of the crucible, sample spacer, and corresponding temperature distribution of the sample.
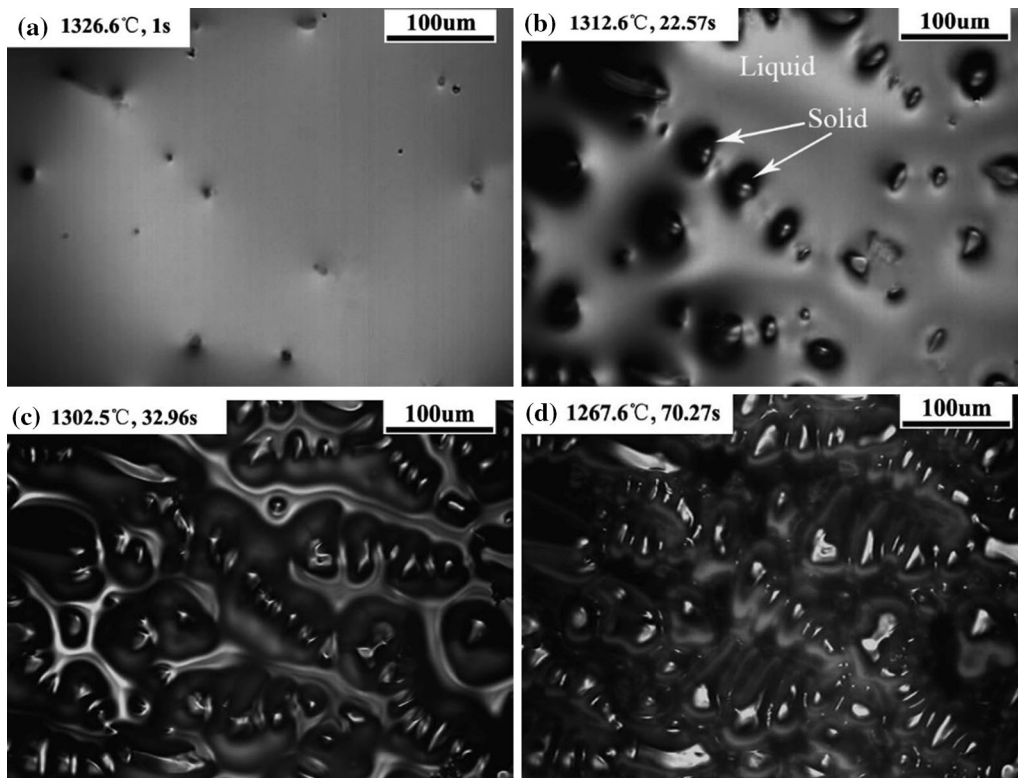

Fig. 2—Typical photos in the solidification at the cooling rate of 1 K/s recorded by HT-LCSM: (a) 1599.6 K (1326.6 °C) and 22.57 s, (b) 1585.6 K (1312.6 °C) and 22.57 s, (c) 1575.5 K (1302.5 °C) and 32.96 s, and (d) 1540.6 K (1267.6 °C) and 70.27 s.

decreasing the temperature, the solid phase, as marked in Figure 2(b), continuously grows and extends into the interdendritic regions. After the formation of dendrite skeleton, the segregation of solute elements such as Nb and Mo exists in the interdendritic areas, which results in nonequilibrium eutectics. The interdendritic regions are the possible positions for the formation of Laves phase. Unfortunately, the formation of Laves phase in interdendritic regions cannot be observed owing to the present capability of HT-LCSM.

The variation of the instantaneous solid fraction, f_s, with solidification time, as shown in Figure 3, can be
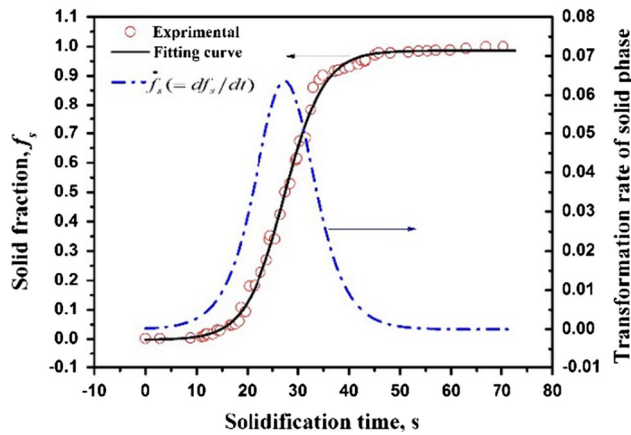
Fig. 3—Solid fraction and transformation rate of solid phase as a function of solidification time at a cooling rate of 1 K/s.
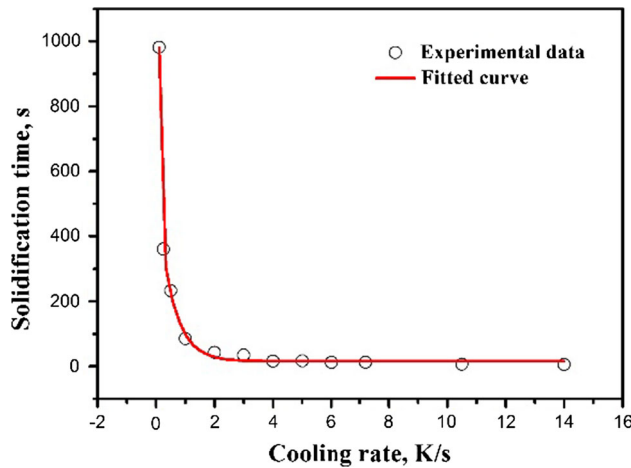

Fig. 4—Solidification time as a function of cooling rate.

acquired by calculating the fraction of solid area in each photograph recorded by HT-LCSM. It is seen that the solidification process accompanying the solute redistribution can be divided into three stages: the initial transient stage, the rapid growth stage, and the final transient stage. The differentiation on the fitted curve of the solid fraction with respect to solidification time displays the transformation rate of the solid phase, $\dot{f}_s = \mathrm{d}f_s/\mathrm{d}_t$, as shown in Figure 3. It shows that the transformation rate of the solid phase presents a feature of Gaussian distribution, which initially increases until a maximum value with a decrease in temperature, gradually decreasing to zero at the final solidification.

For real isothermal solidification, it is hard to precisely acquire the difference between the equilibrium and nonequilibrium solidification temperature ranges at different cooling rates. As a result, the exact relationship between the solidification time and cooling rate largely depends on the experimental conditions. As discussed previously, the transformation rate of solid phase as a function of solidification time at certain cooling rates can be obtained by *in-situ* observations using HT-LCSM in this study. The solidification time at certain cooling rates corresponds to the time range between initial and final zero points of the transformation rate of solid phase, as shown in Figure 3. The relationship of the real solidification time, t_f, with the different cooling rates, $\dot{T}$, in 0.10 to 14 K/s is shown in Figure 4. It can be seen that the solidification time rapidly declines with an increase in the cooling rate below 2 K/s and then almost remains even. These experimental data can been well fitted using a second-order exponential decay function as

$$t_f = 15.66 + 532.38 \exp\left(-\dot{T}/0.538\right) \\ + 6058.14 \exp(-\dot{T}/0.04). \qquad [1]$$

B. Solidification Microstructure

According to the phase diagram, the INCONEL718 alloy solidified under the equilibrium condition is free of Laves phase. However, due to the incomplete diffusion processes in the solid and liquid during nonequilibrium solidification, the alloy elements will be segregated and produce nonequilibrium secondary phase. Typical microstructures of the HT-LCSM sample solidified at a cooling rate of 1 K/s are presented in Figure 5. It can be seen that the solidification microstructure is well-developed equiaxed dendrite and the microsegregation exists among the secondary dendrites, as shown in Figure 5(a). In the interdendritic microsegregation areas, many white blocky, flower-petal-shaped, and skeletal phases coexist, as shown in Figure 5(b). The chemical compositions of these phases and the dendrite core measured by EDS are presented in Table II. It is evidenced that the white blocky and flower-petal-shaped phases enriched with Nb and Mo are primary and eutectic Laves phases, respectively, and the skeletal phase enriched with Nb, Ti, and C is carbide. The skeletal carbides are spatially separated with Laves phase. As a result, the center of the γ dendrites is depleted in Nb, Mo, and Si, but enriched in Fe and Cr. These observations of secondary phases in the interdendritic areas by SEM coincide with the preceding results by HT-LCSM, as shown in Figure 2.

Figure 6 shows the microstructure of HT-LCSM samples solidified at six typical cooling rates. Rough blocky Laves phase with size of ~20- to 30-μm precipitates along the grain boundaries at a low cooling rate of 0.1 K/s. With an increase in the cooling rate, the morphology of the Laves phase in interdendritic areas is changed into flower-petal-shaped and then into small particles, and the size of the Laves phase is continuously reduced. However, the number of Laves phase is increased in a linear relationship with the cooling rates, as shown in Figure 7. As a result, the amount of Laves phase in the HT-LCSM samples as a function of cooling rates is shown in Figure 8. It is interesting to note that the relationship between the cooling rate and Laves phase fraction is that the amount of Laves phase increases in the range of cooling rates slower than 3 K/s and then decreases in the range of 3 to 14 K/s. The maximum of the Laves phase fraction appears at a cooling rate of ~3 K/s.
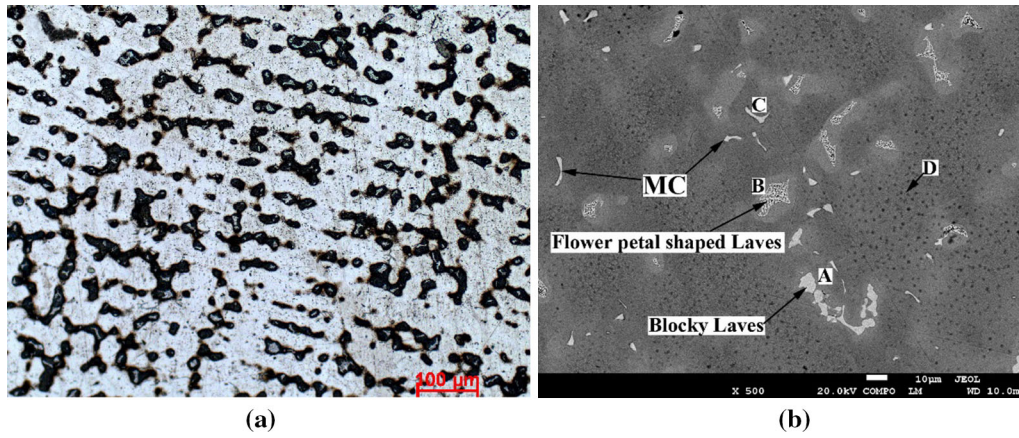
(a)   **(b)**

Fig. 5—Solidification microstructure of the sample at a cooling rate of 1 K/s: (*a*) optical micrograph and (*b*) scanning electron micrograph.

Table II.   Chemical Compositions of Typical Locations in Solidified HT-LCSM Sample (Weight Percent)

Elements	Al	Si	Ti	Cr	Fe	Ni	Nb	Mo	C
Nominal	0.41	0.189	1.06	19.45	18.58	52.09	4.82	3.15	0.06
Spot A	0.29	0.41	0.80	10.38	16.33	34.47	30.56	6.76	—
Spot B	0.35	0.53	1.34	10.80	19.18	38.62	23.86	5.32	—
Spot C	—	—	5.57	2.05	1.06	3.99	58.18	1.86	27.28
Spot D	0.55	—	0.82	18.38	27.23	47.14	2.58	3.31	—

The SDAS, an important parameter in solidification microstructure, indicates the diffusion distance in solidification, which directly determines the microsegregation and amount of Laves phase. Kattamis et al.[21] proposed a simple model to predict the final SDAS (λ_2) based on a coarsening mechanism similar to the Ostwald ripening phenomenon, wherein the growth of a dendrite takes place by the dissolution of smaller dendrites in the melt as follows:

$$\lambda_2 = M\dot{T}^{-n}, \qquad [2]$$

where M is an alloy-dependent parameter and n is the coarsening exponent generally accepted as 1/3.[22–25] However, the M and n are largely decided by the variation of compositions and cooling rates.[25,26] The SDAS results of each HT-LCSM sample measured using the linear intercept method are shown in Figure 9. It is seen that the dendrites are refined with an increase in the cooling rate, as shown in Figure 6, and the fitted curve of SDAS as a function of the cooling rates in the form of Eq.[2] can be expressed as

$$\lambda_2 = 62.9\dot{T}^{-0.407}. \qquad [3]$$

C. Relationship Between the Microsegregation and Laves Phase and Cooling Rate

Among many models concerning dendrite growth and solute segregation in solidification, Nastac proposed a model for equiaxed dendritic solidification, which considers the solute diffusion in both solid and liquid and the effect of thermal, solutal, and curvature undercooling on dendritic growth.[15] Based on the proposed model, a dimensionless microsegregation index (MSI) in terms of the driving forces for diffusion in the liquid and back diffusion in the solid was defined to characterize the microsegregation in an equiaxed dendritic solidification as[16]

$$\mathrm{MSI} = \frac{\mathrm{P_c}}{k\alpha} = \frac{1}{2kD_lD_s}\frac{VL^3}{t_f}, \qquad [4]$$

where $\mathrm{P_c}$ is the solute Péclet number in the liquid, α is the solute Fourier number in the solid, k is the partition coefficient ($k_{Nb} = 0.48$ in INCONEL718), D_l is the diffusion coefficient in liquid ($D_{l,\,Nb} = 3 \times 10^{-9}$ m^2/s), D_s is the diffusion coefficient in solid ($D_{s,\,Nb} = 2.82 \times 10^{-13}$ m^2/s), V is the solidification velocity, and L is the diffusion length.

It should be pointed out that the MSI criterion proposed by Nastac was based on spherical dendrite solidification, where it is considered that the equiaxed dendritic grains grow within a spherical closed system and the grain radius is the characteristic diffusion length. In this study, the solidification microstructure is well-developed equiaxed dendrite and the microsegregation exists among the secondary dendrite arms, as shown in Figure 5. During the end of solidification after the formation of dendrite skeleton, the characteristic back-diffusion distance is half of SDAS for the dendrite growth with secondary branching for an isothermal solidification, as shown in Figure 5(a). Therefore, the diffusion length is adopted as half of the SDAS in this work, and the local solidification velocity is defined as
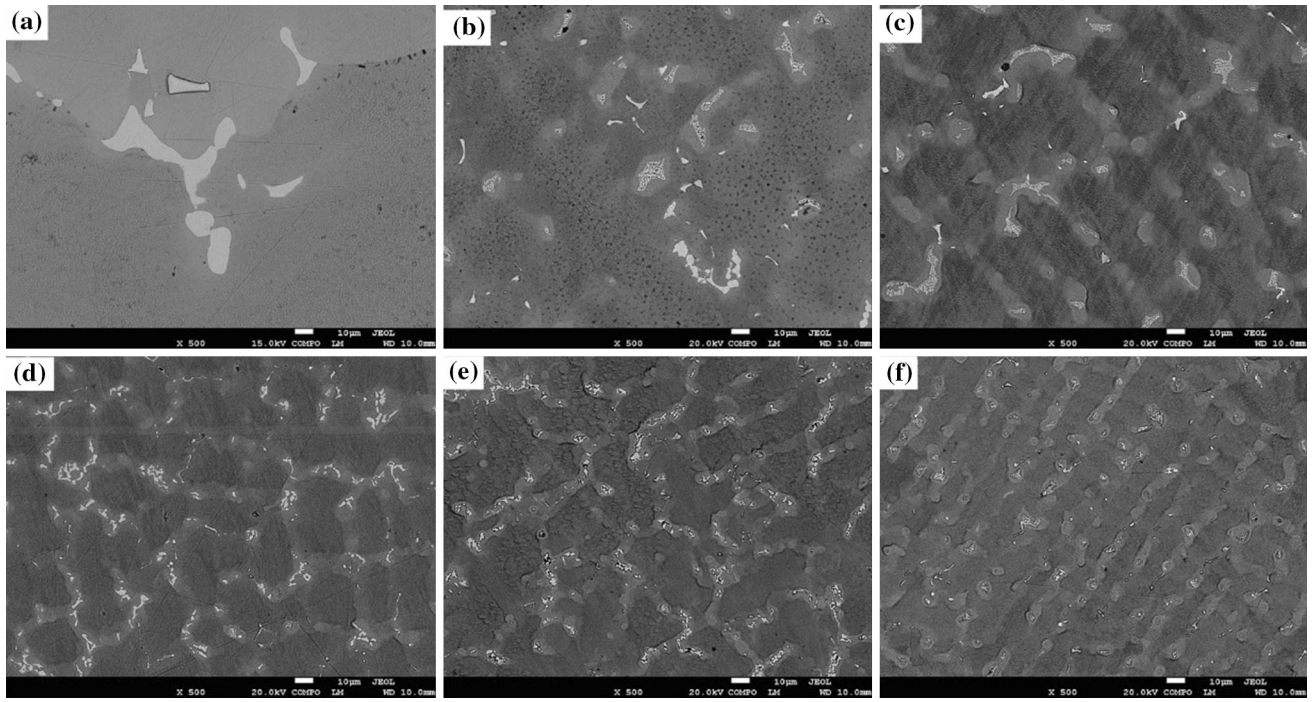
$$V = \lambda_2/2t_f. \qquad [5]$$

Fig. 6—Typical microstructures and Laves morphology evolution of the samples solidified at different cooling rates. (*a*) 0.1 K/s, (*b*) 1 K/s, (*c*) 2 K/s, (*d*) 4 K/s, (*e*) 7 K/s, and (*f*) 14 K/s.
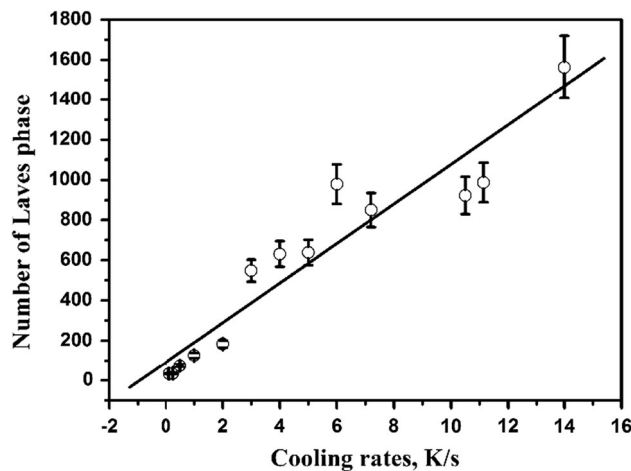

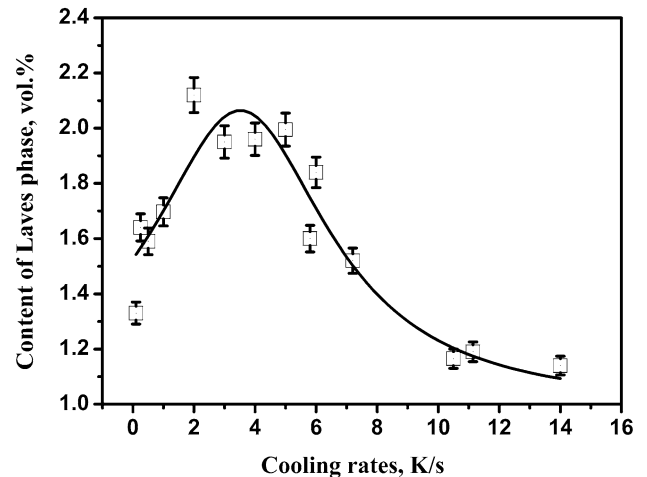Fig. 7—Number of Laves phase as a function of cooling rate.

Fig. 8—Amount of Laves phase as a function of cooling rate.

Accordingly, a modified dimensionless microsegregation index (MMSI) is extended into Eq.[6] based on the MSI criterion proposed by Nastac:

$$\text{MMIS} = \frac{1}{32kD_{\text{L}}D_{\text{S}}} \frac{\lambda_2^4}{t_{\text{f}}^2}. \qquad [6]$$

It is indicated that MMSI is simplified as a function of the SDAS and solidification time when the incorporated material parameters are constant. The SDAS and solidification time have been analyzed and given as functions of the cooling rate in Eqs. [1] and [3],

respectively. Correspondingly, the MMSI as a function of cooling rate is presented in Figure 10. It is shown that the influence of cooling rate on MMSI is the combined effects on the SDAS and solidification time. The MMSI reaches a maximum at a cooling rate of 2.8 K/s, which indicates the maximum of microsegregation. At cooling rates larger than 2.8 K/s, the MMSI increases with increasing cooling rate. Afterward, the MMSI decreases with increasing cooling rate. Since the microsegregation and Laves phase coexist, the amount of Laves phase is the scaling of microsegregation. The prediction of maximal microsegregation by MMSI is consistent with the experimental results of Laves phase content, as shown in Figure 11.
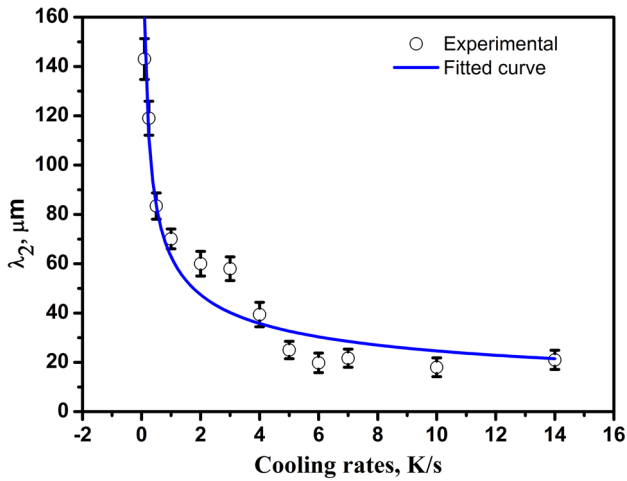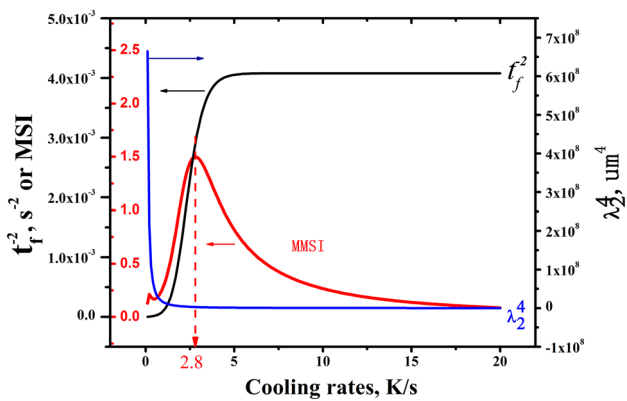
Fig. 9—SDAS as a function of cooling rate.

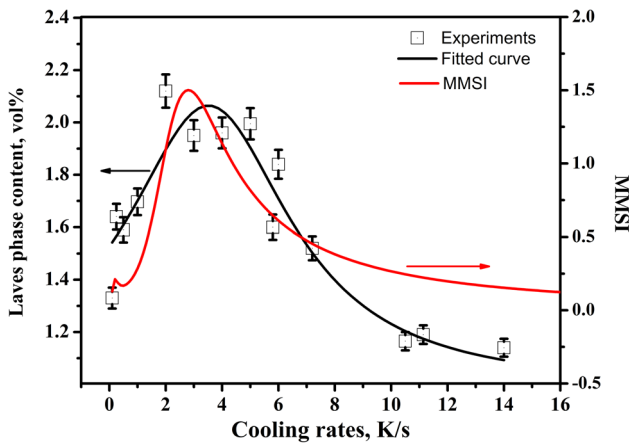Fig. 10—MSI values as a function of cooling rate.

Fig. 11—Comparisons between the Laves phase fraction and MSI values as a function of cooling rate.

The existence of a threshold cooling rate at which the maximal microsegregation and amount of Laves phase are formed, as presented in Figures 8 and 11, is of practical importance for the manufacturing of complex structural casting of INCONEL718. By avoiding the threshold cooling rate using proper process parameters,

the microsegregation and Laves phases in the components should be alleviated.

IV. CONCLUSIONS

1. The transformation rate of solid phase with a feature of Gaussian distribution in the solidification of INCONEL718 superalloy at cooling rates of 0.10 to 14 K/s was acquired by *in-situ* observations with HT-LCSM. The relationship between the solidification time, t_f, and the cooling rate, $\dot{T}$, was obtained and well fitted with a second-order exponential decay function as $t_f = 15.66 + 532.38\exp(-\dot{T}/0.538) + 6058.14\exp(-\dot{T}/0.04)$.

2. With increasing the cooling rate, the SDAS and size of Laves phase in the interdendritic areas were continuously reduced in the solidification microstructures. The SDAS, λ_2, as a function of cooling rate was experimentally evidenced as $\lambda_2 = 62.9\dot{T}^{-0.407}$. The amount of Laves phase reached a maximum at a threshold cooling rate of 3 K/s.

3. An MMSI was used for the scaling of solute segregation and Laves phase depending on the cooling rate. The prediction of maximal microsegregation and amount of Laves phase at the cooling rate of 2.8 K/s by MMSI coincides with the experimental results. The microsegregation and Laves phases in the castings should be alleviated by avoiding the threshold cooling rate, 3 °C/s, using proper process parameters in the applications.

REFERENCES

1. http://www.specialmetals.com/documents/Inconel%20alloy%20718.pdf.
2. D. Furrer and H. Fecht: *JOM*, 1999, vol. 51, pp. 14–17.
3. T.M. Pollock and S. Tin: *J. Propul. Power*, 2006, vol. 22, pp. 361–74.
4. M.D. Kang, H.Y. Gao, J. Wang, L.S.B. Ling, and B.D. Sun: *Materials*, 2013, vol. 6, pp. 1789–1802.
5. B. Seiser, R. Drautz, and D.G. Pettifor: *Acta Mater.*, 2011, vol. 59, pp. 749–63.
6. N. Zhou, D.C. Lv, H.L. Zhang, D. McAllister, F. Zhang, M.J. Mills, and Y. Wang: *Acta Mater.*, 2014, vol. 65, pp. 270–86.
7. G.A. Knorovsky, M.J. Cieslak, and T.J. Headley: *Metall. Trans. A*, 1989, vol. 20A, pp. 2149–58.
8. L. Nastac: *Acta Mater.*, 1999, vol. 47, pp. 4253–62.
9. J.N. DuPont, C.V. Robino, and A.R. Marder: *Acta Mater.*, 1998, vol. 46, pp. 4781–90.
10. L. Wang, Y. Yao, J. Dong, and Z. Maicang: *Chem. Eng. Commun.*, 2010, vol. 197, pp. 1571–85.

11. T.F. Bower, H.D. Brody, and M.C. Flemings: *Trans. TMSAIME*, 1966, vol. 236, pp. 624–33.
12. M.C. Flemings: *Metall. Trans.*, 1974, vol. 5, pp. 2121–34.
13. T. Antonsson and H. Fredriksson: *Metall. Mater. Trans. B*, 2005, vol. 36B, pp. 85–96.
14. L. Nastac and D.M. Stefanescu: *Metall. Mater. Trans. A*, 1997, vol. 28A, pp. 1582–87.
15. L. Nastac and D.M. Stefanescu: *Metall. Mater. Trans. A*, 1996, vol. 27A, pp. 4061–74.
16. L. Nastac and D.M. Stefanescu: *Metall. Mater. Trans. A*, 1996, vol. 27A, pp. 4075–83.
17. H. Yin and T. Emi: *Metall. Mater. Trans. B*, 2003, vol. 34B, pp. 483–93.
18. D. Phelan, M. Reid, and R. Dippenaar: *Metall. Mater. Trans. A*, 2006, vol. 37A, pp. 985–94.
19. P.T. Jones, D. Desmet, M. Guo, D. Durinck, F. Verhaeghe, J.V. Dyck, J. Liu, B. Blanpain, and P. Wollants: *J. Eur. Ceram. Soc.*, 2007, vol. 27, pp. 3497–3507.
20. M.M. Attallah, H. Terasaki, R.J. Moat, S.E. Bray, Y. Komizo, and M. Preuss: *Mater. Characterization*, 2011, vol. 62, pp. 760–67.
21. T.Z. Kattamis, J.C. Coughlin, and M.C. Flemings: *Trans. TMS-AIME*, 1967, vol. 239.
22. M.C. Flemings: *Mater. Trans.*, 2005, vol. 46, pp. 895–900.
23. V.R. Voller and C. Beckermann: *Metall. Mater. Trans. A*, 1999, vol. 30A, pp. 3016–19.
24. V.R. Voller: *Int. J. Heat Mass Transfer*, 2000, vol. 43, pp. 2047–52.
25. J.L. Fife and P.W. Voorhees: *Acta Mater.*, 2009, vol. 57, pp. 2418–28.
26. Q. Du, D.G. Eskin, A. Jacot, and L. Katgerman: *Acta Mater.*, 2007, vol. 55, pp. 1523–32.
27. M. Paliwal and I.H. Jung: *Acta Mater.*, 2013, vol. 61, pp. 4848–60.